Pergamon

Int. J. Heat Mass Transfer. Vol. 38, No. 3, pp. 533–543, 1995

0017-9310/95 $9.50+0.00

0017-9310(94)00171-5

Experiments on natural convection from two staggered vertical plates

GIOVANNI TANDA

Dipartimento di Termoenergetica e Condizionamento Ambientale, Università di Genova, via all'Opera Pia 15/a, I-16145 Genova, Italy

(*Received* 17 *February* 1994)

Abstract—The thermal field and the heat transfer characteristics of a system consisting of two staggered vertical plates cooled by air in free convection were experimentally studied. The parameters investigated included the interplate spacing, the magnitude of the vertical stagger, and the Rayleigh number based on the overall convective heat flux from each plate. The experiments were performed in air. The schlieren optical technique was employed to obtain the thermal field around the plates and the local heat transfer coefficients along the vertical sides of plates. Staggering was found to markedly affect the local heat transfer characteristics of the facing sides of the plates when the interplate distance was relatively small. In general, the Nusselt number averaged on the inner face of the lower plate was enhanced (up to over 40%) compared with that for the case of the unstaggered plate channel. Conversely the mean Nusselt number on the facing side of the upper plate was reduced (up to 15%).

INTRODUCTION

Natural convection in vertical channels is encountered in several technological applications, such as electronic equipment, cooling and passive solar heating systems. Since the pioneering works of Elenbaas [1, 2] in the 1940s, this topic has been studied extensively by many authors. Theoretical, numerical and experimental works dealing with the effects of the heating mode (symmetrical or asymmetrical, at uniform heat flux or at uniform wall temperature), the air inlet conditions and the radiant exchange can be found in the literature (see refs. [3–7] for instance). Useful relationships giving the Nusselt numbers and the optimum plate spacings for the various boundary conditions are presented in ref. [8].

The use of staggered, discrete, vertical plates, as an alternative to continuous, parallel, vertical plates has been proposed, in recent years, in order to achieve heat transfer enhancement in systems (such as finned surfaces and printed circuit boards) cooled in free convection. The first study on natural convection from staggered vertical plates involved the experiments reported in ref. [9]. Some years later, the heat transfer performance of a staggered array of discrete vertical plates was numerically evaluated and compared with that of an array of continuous parallel vertical plates [10] and of an array of in-line discrete vertical plates [11], under given constraints. Computations performed in wide fields of variation of parameters revealed that the use of discrete plates (both staggered and in-line) in lieu of continuous plates gives rise to heat transfer enhancement (up to a factor of two). While in refs. [10, 11] a two-dimensional problem with zero plate thickness and no fluid recirculation was tackled, a more practical situation, involving an assembly of vertical staggered segments of finite length and thickness (connected to an isothermal baseplate) was experimentally investigated in ref. [12], in which a general correlation for natural convection heat transfer is presented. Convective interactions between two staggered plates were numerically evaluated in refs. [13, 14], while experiments on a four-staggered-plate array were recently presented in ref. [15].

The present work is seemingly the first to experimentally investigate natural convection from two staggered vertical plates. This configuration can be encountered in the packaging of electronic devices such as printed circuit boards and thus may be of practical interest for designers. In addition, information concerning the thermal field and local heat transfer characteristics, even though limited to a two-plate array, contributes to the fundamental understanding of convective interactions in staggered plate configurations.

The study was performed in air. The parameters investigated consisted of the interplate spacing, the magnitude of the staggering, and the overall convective heat flux exchanged by each plate. Emphasis is placed on the influence exerted by the vertical staggering on heat transfer from the facing sides of the two plates. An apparatus based on the schlieren optical technique was used to perform a non-intrusive analysis of the thermal field as well as the local heat transfer characteristics.

EXPERIMENTS

Apparatus

The experimental apparatus consists of two staggered vertical plates, a power supply system, a

NOMENCLATURE

A	vertical stagger magnitude
c_p	specific heat at constant pressure of the fluid
D	plate thickness
g	acceleration of gravity
H	plate height
h	local natural convection heat transfer coefficient
k	thermal conductivity of the fluid
L	plate length
Nu	local Nusselt number
$\overline{Nu}$	average Nusselt number
Q_c	per-plate convective heat transfer rate
Ra	Rayleigh number
S	interplate spacing
T	absolute temperature
x, y, z	spatial coordinates.

Greek symbols

α	light ray angular deflection
β	coefficient of thermal expansion of the fluid
Δ	light ray deviation
μ	dynamic viscosity of the fluid
ρ	density of the fluid
ϑ	dimensionless temperature
Ω	constant in equations (1), (2), (4).

Subscripts

1, 2	lower and upper plate, respectively
i	inner side of plate
w	wall conditions
∞	ambient conditions.

schlieren optical system, and instruments for measuring temperature, electrical power and pressure. The two vertical plates, suspended by nylon lines, were located at different levels (with a vertical stagger A) and separated by a space S, as shown in Fig. 1. The dimensions of each plate are as follows: thickness $D = 8$ mm, height $H = 6.5$ cm, and length (in the third dimension) $L = 30$ cm. The length was chosen as much greater than the other dimensions in order to favor a two-dimensional thermal field around the heated plates. Each plate consists of two aluminum sheets and a plane electrical resistance sandwiched between them to dissipate the power input by the Joule effect (Fig. 2). Both the plates and the surroundings were instrumented with fine-gage, chromel–alumel thermocouples, calibrated to ± 0.1 K. Six to 10 thermocouples were embedded in the wall of each plate at different locations through 0.5-mm dia. holes drilled into the rear surfaces of the two coupled aluminum sheets (see details in Fig. 2). Care was taken to drill the hole as close to the exposed surfaces as possible. The ambient air temperature was measured by five shielded thermocouples situated just below the plate array.

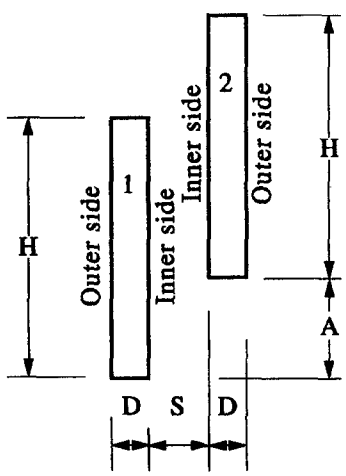

Fig. 1. Schematic layout of the two staggered vertical plates.

The power input supplied to each plate was transferred to the surroundings by natural convection and radiation. Since the thermal resistance of the plate material was very small, owing to the high thermal conductivity of aluminum, each plate was expected to be virtually isothermal. Surface temperature uniformity was checked by means of an infrared thermographic system in a preliminary experiment. The wall temperature field on a single heated plate (previously black-anodized to increase thermography sensitivity) was analyzed. The maximum temperature nonuniformities, based on the mean plate-to-ambient temperature difference, turned out to be 1% in the vertical direction and 4% in the transverse direction. In particular, a 2% temperature drop was found in proximity to the transverse ends of the plate (within approx. 2 cm of the edges), due to limited three-dimensional effects. The same wall temperature behavior was expected in the experiments on the two-plate system, for which the maximum variations over each plate (recorded by the deployed thermocouples) were generally less than 2% of the plate-to-ambient temperature difference. Hence, each plate was assumed to attain a different uniform surface temperature, depending on the characteristics of the buoyancy-induced flow and on the amount of heat power to be transferred to the surroundings.

As previously noted, all of the heating power supplied to a given plate was dissipated at its exposed surfaces by natural convection and radiation. The radiation heat transfer was reduced to a small value (less than 10% of the total power input), because of

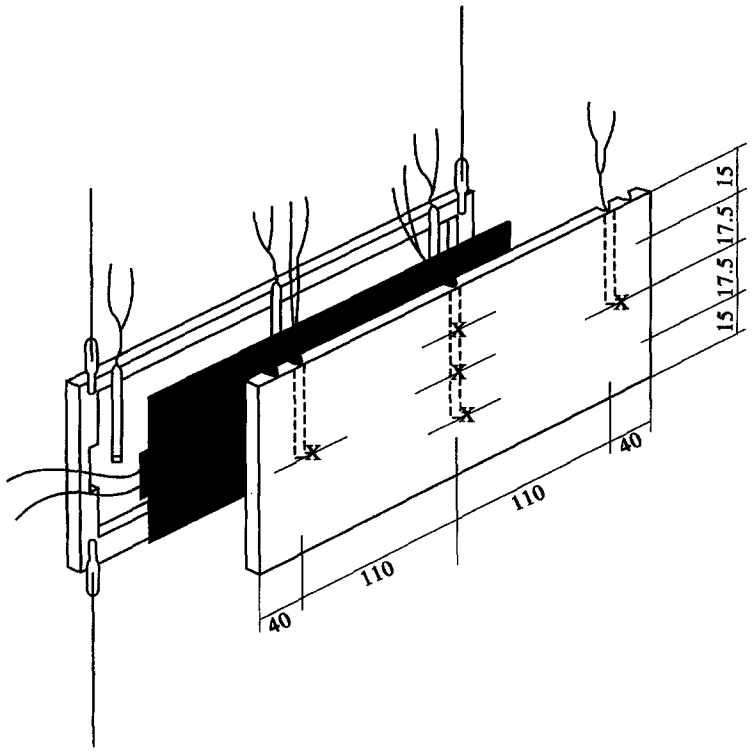

Fig. 2. Detail of the housing of electrical heater and thermocouples (X) in the plate.

the low thermal emittance of aluminum surfaces, which was measured by a radiometric apparatus as 0.1 ± 0.02 in the temperature range of interest. The radiation heat transfer from each plate was accurately determined by calculation, using the net-radiation method for enclosures of diffuse-gray surfaces, and subtracted from the total power input, thereby yielding the per-plate natural convection heat transfer rate Q_c.

The plate assembly was confined on four sides by glass walls with open grids at the bottom. Runs conducted without the side walls revealed negligible effects on heat transfer performance, but the walls were deemed necessary to minimize extraneous air-current effects that might disturb the optical measurements.

A schlieren optical system was employed to reconstruct the thermal field and to perform measurements of local heat transfer coefficients. The schlieren system is schematically shown in Fig. 3a. A non-coherent light beam from a vertical slit source, collimated by the concave mirror M_1, passes through the test section. A second concave mirror M_2 is then used to form a real image of the slit source in the focal plane and a real image of the test section onto a screen or camera. Owing to the inhomogeneities of the fluid refractive index around plates, the light rays undergo angular deflections. Regions of the optical field that have the same light deflection α (or the same light deviation Δ) can be identified by shifting an opaque vertical filament in the focal plane of mirror M_2, as shown in Fig. 3b. When a disturbed light ray is stopped by the focal filament, the image of the corresponding region of fluid will appear dark on the screen, while the remaining field will be bright. The deviation Δ of a disturbed ray in the focal plane of mirror M_2 can be recorded by measuring the distance between the middle of the undisturbed image of the slit source and the centerline of the filament, i.e. the distance between the filament positions 1 and 2 displayed in Fig. 3b. If the thermal field is assumed to be two-dimensional (i.e. temperature is independent of z-coordinate), the shift Δ of each light ray (due to the deflection in the y–z plane) can be related to the local temperature gradient by the relationship,

$$\Delta = \Omega \cdot (\partial T/\partial y)/T^2 \tag{1}$$

where $T = T(x, y)$ is the absolute temperature, y is the direction in which the light deflection is recorded and Ω is a constant depending on the fluid, the pressure, the plate length and geometric parameters of the optical components. In the present experiment, Ω was equal to -0.0456 m^2 K. The temperature reconstruction procedure is based on a set of photographs (for each experimental run) obtained with the focal filament placed at different distances Δ from the undisturbed slit-source image. A typical example of a photograph taken by the schlieren apparatus is reported in Fig. 4. By identifying for each photograph the coordinates of the centerline of the filament shadow, it is possible to obtain the profile of lines of constant light-deviation values Δ and thus, taking into

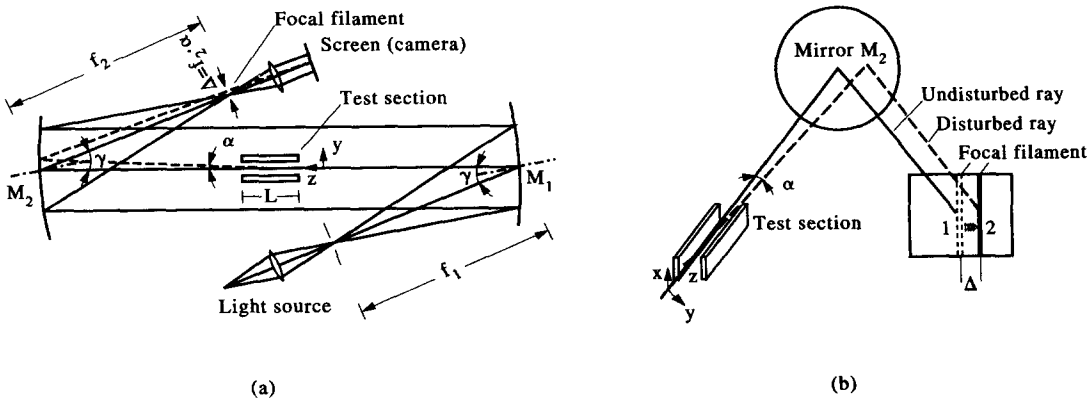

Fig. 3. (a) Schlieren apparatus (top view): M_1 and M_2 are 0.38-m dia. concave mirrors (with focal lengths f_1 and f_2, respectively), α is the angular deflection of the light ray (in the y–z plane) and Δ is the corresponding light deviation at the focal plane of mirror M_2 ($f_1 = f_2 = 1.9$ m, $\gamma = 9°$, distance between mirrors about 8 m). (b) Measurement of light deviation Δ at the focal plane of mirror M_2: the focal filament is shifted from position 1 to position 2.

account equation (1), reconstruct the temperature distribution in the entire optical field.

The local heat transfer coefficient can be directly obtained from schlieren images without having to reconstruct the whole thermal field. Indeed, if the focal filament is moved until its shadow intersects (in the image projected on the camera) the vertical surface profile, the displacement of the filament corresponds to the deviation Δ_w of the light ray passing in the vicinity of the wall at the desired location. The relation between light deviation Δ_w and the local heat transfer coefficient can be easily shown as follows. By applying equation (1) at the heated walls, one obtains

$$\Delta_w = \Omega \cdot (\partial T/\partial n)_w / T_w^2 \tag{2}$$

where $(\partial T/\partial n)_w$ is the temperature gradient in the direction normal to the plate surface, evaluated at the wall, and T_w is the wall temperature. By introducing the definition of local heat transfer coefficient

$$h = \frac{-k_w(\partial T/\partial n)_w}{(T_w - T_\infty)} \tag{3}$$

where k_w is the thermal conductivity of the fluid at the wall temperature and T_∞ is the ambient air temperature, it follows that

$$h = -k_w \Delta_w T_w^2 / (\Omega (T_w - T_\infty)). \tag{4}$$

Further details on the derivation of fundamental schlieren formulae (1, 2), as well as on the thermal field reconstruction procedure, are given in refs. [15, 16].

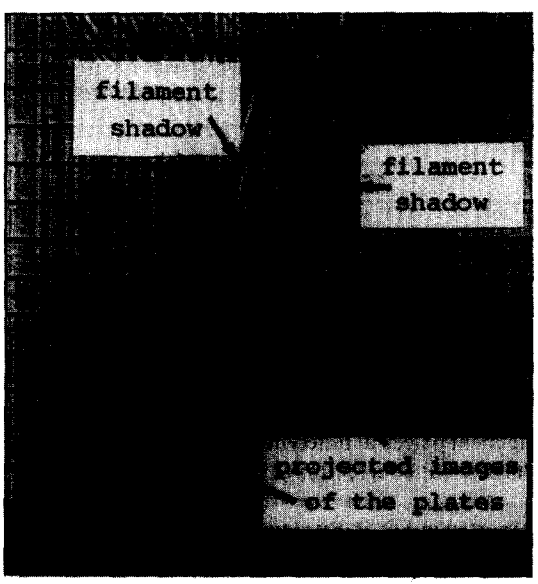

Fig. 4. Schlieren image recorded for $S/H = 0.23$, $A/H = 0.38$, $Ra = 3.0 \times 10^7$, $\Delta = 0.7$ mm.

Operating procedure

Experimental runs were performed according to the following procedure:

(i) Arrangement of the plate configuration, by setting proper values of the interplate spacing S and of the staggering magnitude A. Dimensionless quantities S/H and A/H represent the geometric parameters of the configuration, ranging between 0.09 and 0.46 and between 0.0 and 1.0, respectively. Obviously, for A/H equal to zero, the configuration coincides with the unstaggered parallel plate channel. It should be noted that values of S/H equal to about 0.09–0.10 correspond to the optimum spacings which maximize the heat flux from an array of isothermal unstaggered vertical plates [8], and therefore modifications in heat transfer characteristics due to staggering at these S/H values may have an important practical significance.

(ii) Heating of the plates by a given input of electrical power into the heaters. By subtracting the calculated radiant heat transfer rate from the electrical power, each plate dissipates a controlled overall free-convection heat transfer rate Q_c at its exposed surfaces. Experimental runs were conducted by keeping the overall convective heat transfer rates from both plates equal. Values of Q_c were 7, 11 and 15

W per plate, respectively; the corresponding wall-to-ambient temperature differences ranged from 25 to 51 K, depending on the selected value of Q_c and the specific position of the plate.

(iii) In the steady state, measurements of wall and ambient air temperatures and, for a number of experiments, reconstruction of the thermal field from a set of schlieren photographs (from 10 to 20 for each run).

(iv) Optical measurement of the light deflections near the vertical walls in order to obtain the local heat transfer coefficients at several locations along the plate surfaces.

In addition, further experiments were performed for a single heated plate, this case corresponding to $S/H \Rightarrow \infty$ or $A/H \Rightarrow \infty$ limiting conditions.

As previously done for geometric parameters S and A, measured data were recast in a dimensionless form by introducing Rayleigh and Nusselt numbers and a scale temperature function:

$$Ra = c_p \rho^2 g \beta H^3 (Q_c/L)/(k^2 \mu) \quad (5)$$

$$Nu = hH/k \quad (6)$$

$$\vartheta = (T - T_\infty)/(T_{w,2} - T_\infty) \quad (7)$$

where k, β, μ, ρ and c_p represent the thermal conductivity, the thermal expansion coefficient, the dynamic viscosity, the density and the specific heat (at constant pressure) of the fluid, respectively, g is the gravitational acceleration and $T_{w,2}$ is the wall temperature of the (upper) plate 2. When referred either to plate 1 or plate 2, the fluid properties appearing in equations (5, 6) were evaluated at the local film temperatures $T_1^* = (T_{w,1} + T_\infty)/2$ or $T_2^* = (T_{w,2} + T_\infty)/2$. Since the overall convective heat flux exchanged by each plate was the same and T_1^* and T_2^* were very close in the steady state, each experimental run was characterized by a given value of the Rayleigh number for both plates. Conversely, Nusselt numbers were expected to strongly differ from plate 1 to plate 2. Therefore, subscripts 1 and 2 were introduced. The additional subscript i was adopted to denote Nusselt numbers evaluated on the inner sides of each plate (see Fig. 1). The averaged value of local Nusselt numbers was indicated by using a bar over the corresponding symbol.

Uncertainty of results

The uncertainties of the main quantities obtained from the experimental investigation were estimated according to the procedure outlined in ref. [17]. The accuracy of the optical measurements performed is, in general, sensitive to the circumstances involved (dimensions of optical components, length of the perturbed optical path, etc.). The uncertainty in the light deviation Δ_w readings was found to be the main source of error in the local heat transfer coefficient h measurements. Since the accuracy in Δ_w readings improves with increasing Δ_w, the uncertainty in h values turned out to be inversely proportional to the recorded Δ_w values. For the present experiment, the (20/1) uncertainty in the local heat transfer coefficient (or local Nu number) was estimated to range from 20 to 8%, in the field of Δ_w values between 0.8 and 9 mm (in which measurements were performed). Since integration averages the noise in the local Nusselt number values, the average Nusselt number data are likely to be more accurate than the local Nusselt number data. The reproducibility in the average Nusselt number values, assessed by repeating all the experiments over the entire parameter ranges, was found to be always less than 8%. The uncertainty in Ra values turned out to be 5%, while the uncertainty in the reconstructed temperature T was about 2–4% of the maximum wall-to-ambient temperature difference [16], giving a maximum uncertainty of ± 0.04 in ϑ values. Comparison of local heat transfer coefficients measured in the case of an isothermal single vertical plate with prediction of Ostrach [18] revealed a maximum deviation of only 10%. Comparison of local and average heat transfer coefficients obtained for two isothermal unstaggered vertical plates showed a maximum deviation of 9% from the numerical results of Naylor *et al.* (Fig. 5 of ref. [7], spacing-to-height ratio = 1/12), and of 13% from the correlation of Elenbaas [2].

RESULTS AND DISCUSSION

As can be noticed from Fig. 1, the position of the two plates defines a channel, confined between the two facing sides of the plates (denoted as "inner sides"). The height of this channel is reduced with increase in the magnitude of the vertical staggering. The air flow entering the channel is established by a balance between the buoyancy and the friction forces. In this context, the system adjusts itself in accordance with whatever changes have occurred in the interplate spacing, staggering magnitude and Rayleigh number. Therefore, the heat transfer characteristics of the inner sides of plates are expected to be significantly affected by the above parameters. Conversely, the outer sides of plates are likely to be free of interactions, and the corresponding boundary layers are expected to grow as in the single-plate limiting case.

Temperature profiles

The reconstructed temperature distributions for different interplate spacings S/H, staggering magnitudes A/H and elevations x/H, are reported in Figs. 5 and 6. All the results are obtained for $Ra = 3.0 \times 10^7$. Figure 5 shows temperature profiles for $S/H = 0.23$ and $A/H = 0$ and 0.69. In the absence of staggering ($A/H = 0$), the thermal field is clearly symmetrical. The airstream flowing up within the channel formed by the plates is only slightly heated ($\vartheta \approx 0.2$ for $x/H = 0.92$ and $y/H = 0$), since the wall thermal boundary layers remain separated over most of the channel height. As the plates are staggered ($A/H = 0.69$), the thermal plume arising from the lower plate 1 leads to local air temperature peaks at

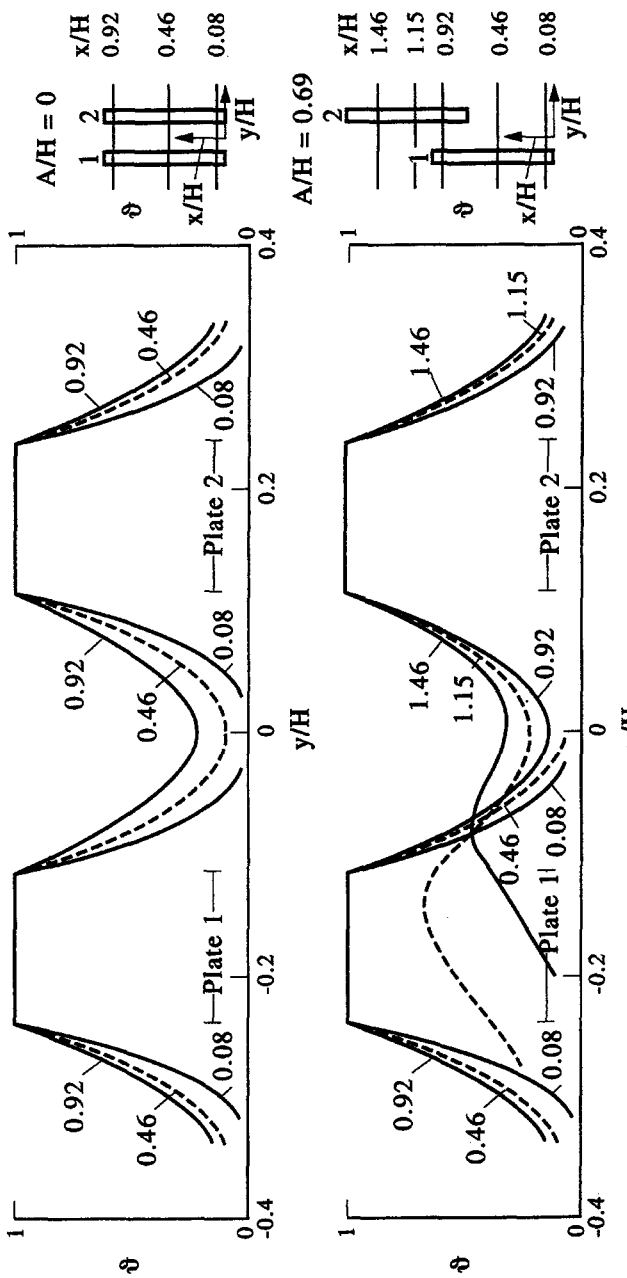

Fig. 5. Dimensionless temperature ϑ distributions at different elevations x/H for $A/H = 0$ and 0.69. $S/H = 0.23$, $Ra = 3.0 \times 10^7$.

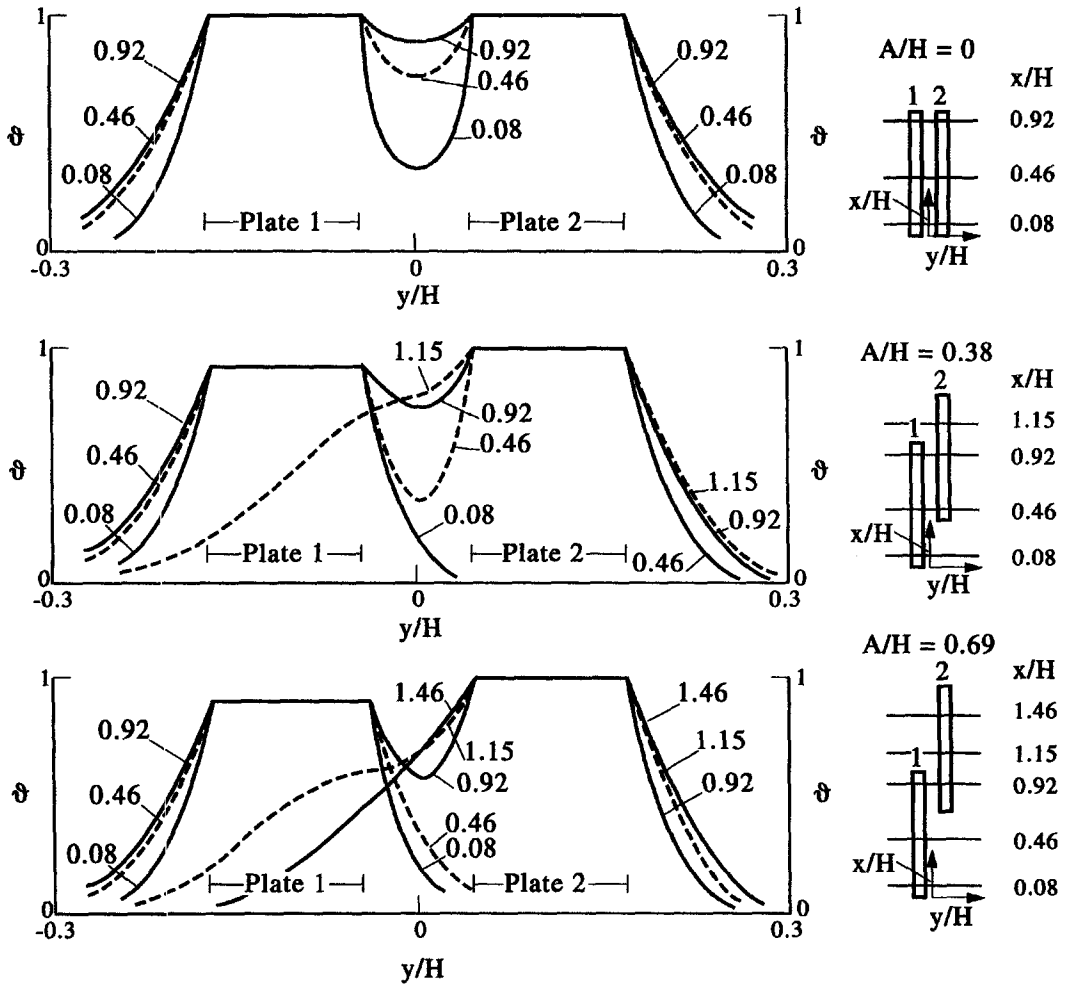

Fig. 6. Dimensionless temperature ϑ distributions at different elevations x/H for $A/H = 0$, 0.38 and 0.69. $S/H = 0.09$, $Ra = 3.0 \times 10^7$.

the highest elevations ($x/H = 1.15$ and 1.46), as one moves away from the inner side of the upper plate 2. The transverse coordinate of this temperature peak seems to move towards the upper plate as the vertical coordinate is increased. Temperature distributions for $S/H = 0.09$, with A/H varying from 0 to 0.38 to 0.69, are plotted in Fig. 6. In this case, when the plates are unstaggered ($A/H = 0$), the thermal boundary layers merge near the entrance owing to the reduced interplate spacing. As a consequence, the air temperature at the channel centerline ($y/H = 0$) reaches very high values ($\vartheta \approx 0.9$ at $x/H = 0.92$). When a nonzero vertical stagger is present, the plates attain different temperature values (the lower plate becomes more efficient, in terms of the heat transfer performance, than the opposite plate as A/H is increased from 0 to 0.69). At the highest elevations (x/H higher than unity), the thermal wake generated by the lower plate blends with the thermal boundary layer growing along the upper plate and loses its identity with increasing x/H. It is worth to notice that the thermal field near the outer sides of plates is practically unchanged by reducing S/H.

Local heat transfer characteristics

The main purpose of this work was to study the modifications in the local heat transfer characteristics due to a staggered displacement of the two vertical plates. This analysis was performed on vertical sides of plates. As previously discussed, staggering the plates is likely to induce modifications in heat transfer performance mainly on the inner sides. This expectation was confirmed by measurements of local heat transfer coefficients along the outer sides of plates, which were generally found to be very close to those for the single-plate case. Only for the reduced interplate spacing $S/H = 0.09$, and for $A/H = 0$, did Nusselt numbers in the lower regions of outer sides turn out to be slightly different (about 10% in excess) from the corresponding values for the single plate. This difference was found to vanish with increasing A/H.

Therefore, attention was mainly devoted to Nusselt

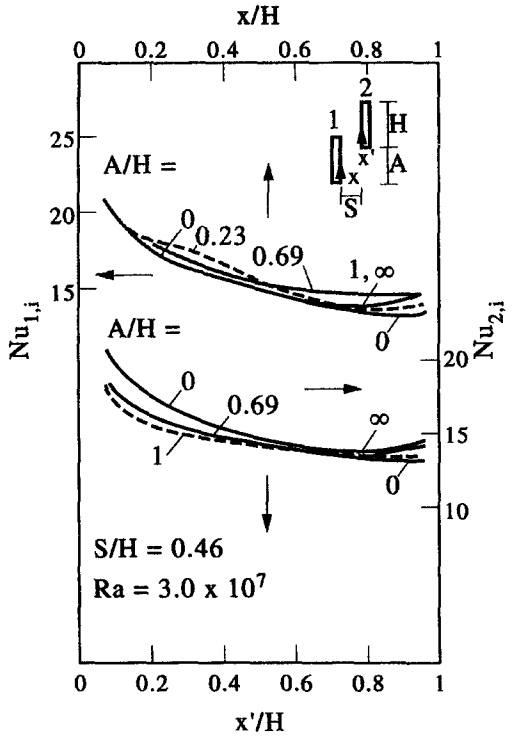

Fig. 7. Distributions of local Nusselt numbers $Nu_{1,i}$ and $Nu_{2,i}$ evaluated along the inner sides of plates 1 and 2 for different values of A/H. $S/H = 0.46$, $Ra = 3.0 \times 10^7$.

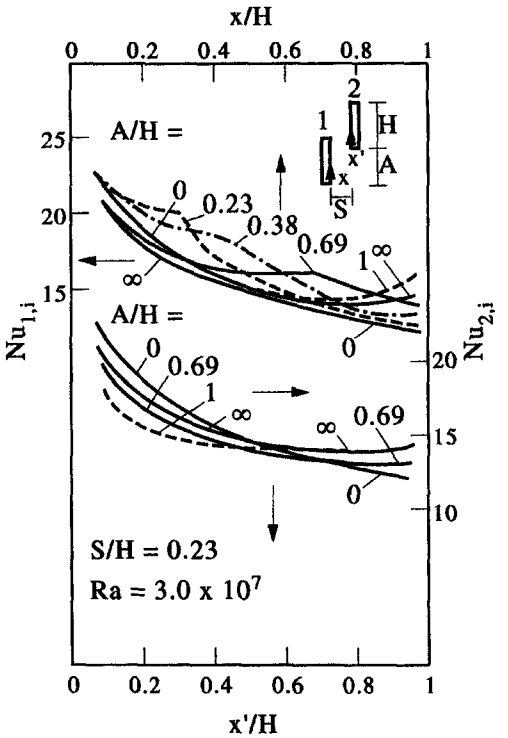

Fig. 8. Distributions of local Nusselt numbers $Nu_{1,i}$ and $Nu_{2,i}$ evaluated along the inner sides of plates 1 and 2 for different values of A/H. $S/H = 0.23$, $Ra = 3.0 \times 10^7$.

numbers $Nu_{1,i}$ and $Nu_{2,i}$ evaluated along the inner sides of plates and presented in Figs. 7–9. When the interplate spacing is relatively large ($S/H = 0.46$, Fig. 7) $Nu_{1,i}$ and $Nu_{2,i}$ profiles are almost insensitive to the degree of stagger. This finding suggests that, with an interplate spacing of this magnitude, Nusselt numbers will not differ significantly from those of the single-plate case in any staggering condition. As the spacing S/H is reduced ($S/H = 0.23$, Fig. 8), the staggered case reveals downside and upside deviations (in the $\pm 10\%$ range) from the results seen in the unstaggered case.

The strongest influence of the staggering on local Nusselt numbers is exerted at $S/H = 0.09$ (Fig. 9). In this case, local Nusselt number distributions are plotted for three values of the Rayleigh number ($Ra = 2.1 \times 10^7$, Fig. 9a, $Ra = 3.0 \times 10^7$, Fig. 9b, and $Ra = 3.7 \times 10^7$, Fig. 9c). When the plates are unstaggered ($A/H = 0$), $Nu_{1,i}$ and $Nu_{2,i}$ profiles coincide and both start from values in excess of those for the single-plate case ($A/H \Rightarrow \infty$), owing to entrance effects. On increasing the vertical coordinate, the opposite boundary layers merge and Nusselt numbers for the unstaggered channel decrease more sharply than those for the single plate.

As the staggering magnitude A/H is increased from 0 to 1, the local Nusselt numbers near the leading edge of both plates drop to below those of the unstaggered configuration. For plate 1 this decrease is related to the reduced velocity of the cooling air (the staggering reduces the air draft), while for plate 2 it is due to the preheating of the up-flowing airstream. In all cases, $Nu_{1,i}$ profiles have a peak at the inlet of the staggered channel ($x/H = A/H$), owing to the flow acceleration caused by the blockage effect of the upper plate, and then drop sharply as the vertical coordinate increases further. $Nu_{2,i}$ values generally decrease with x'/H up to the exit of the staggered channel ($x'/H = 1 - A/H$) and then remain practically unchanged up to the top of the plate ($x'/H = 1$). When the vertical stagger is equal to the plate height ($A/H = 1$), the lower plate exhibits the same Nusselt distributions as the single plate. Conversely, Nusselt number profiles on the upper plate show the same trend as the single plate with 20–30% reductions due to the preheating of the rising air flow. As shown in Fig. 9, Nusselt number results exhibit similar behavior for all the Rayleigh number values here considered; the trend of the local Nusselt number values to increase with increasing Rayleigh number was generally observed.

Average heat transfer characteristics

Attention is devoted at first to Nusselt numbers numerically averaged either on outer or on inner sides of the plates. While Nusselt number values averaged on the outer sides are practically equal to the single-plate values or slightly higher (5% for $S/H = 0.09$ and $A/H = 0$), the Nusselt values averaged on the inner sides fall into a wide range of variation, according to

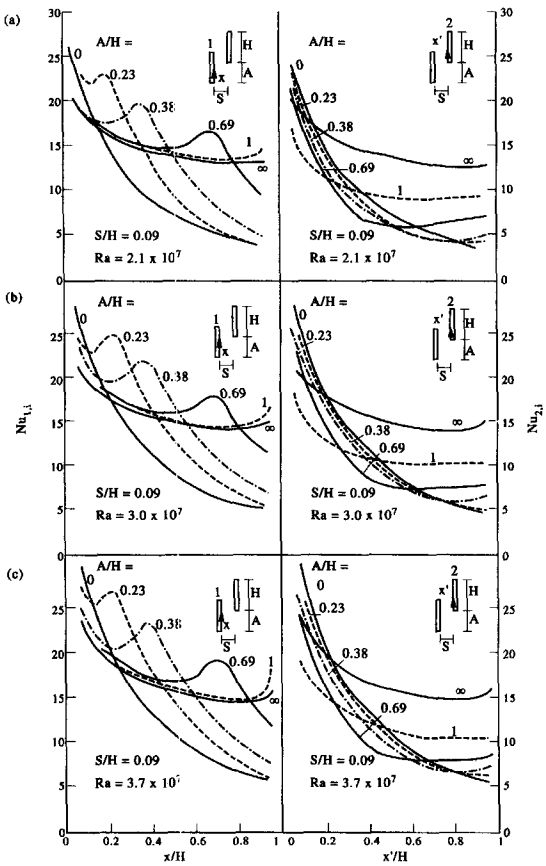

Fig. 9. Distributions of local Nusselt numbers $Nu_{1,i}$ and $Nu_{2,i}$ evaluated along the inner sides of plates 1 and 2 for different values of A/H and Ra. $S/H = 0.09$. (a) $Ra = 2.1 \times 10^7$; (b) $Ra = 3.0 \times 10^7$; (c) $Ra = 3.7 \times 10^7$.

the values assumed by the parameters of the study. In Fig. 10 the Nusselt numbers $\overline{Nu}_{1,i}$ and $\overline{Nu}_{2,i}$, averaged on the inner sides of plates 1 and 2, respectively, are reported as a function of the dimensionless staggering A/H, and for three values of S/H and Ra. Data obtained for a single isothermal vertical plate are also reported, since they are representative of the asymptotic limit $A/H \Rightarrow 0$. For $S/H = 0.46$, the Nusselt numbers averaged on inner sides of plates are only slightly affected by the staggering (within $\pm 6\%$ as compared with values for $A/H = 0$). This result agrees rather well with computations performed in ref. [14], for $S/H = 0.5$ and for a similar Rayleigh number, taking into account the different definition assumed in this paper. For $S/H = 0.23$, appreciable differences between the heat transfer performance of inner faces of plates appear, especially in the range of intermediate A/H values. These differences markedly increase as the interplate spacing is reduced ($S/H = 0.09$). It is worth introducing the Bar Cohen–Rohsenow formula [8],

$$2S_{opt} + 3D - 0.005(c_p \beta g (T_w - T_\infty)\rho^2/\mu k H)^{1.5} S_{opt}^7 = 0 \quad (8)$$

where S_{opt} is the spacing between adjacent plates which yields the maximum rate of heat transfer from an array of unstaggered isothermal vertical plates. If one introduces into equation (8) the thermophysical properties and $T_w - T_\infty$ values obtained in this paper for $A/H = 0$, the relationship is satisfied for S_{opt} equal to about 6–7 mm, i.e. for S/H values very close to 0.09. Therefore, when this spacing value between the unstaggered plates is set, inspection of Fig. 10 reveals that a vertical stagger leads to considerable enhancements (up to over 40%) in inner-side average heat transfer coefficients of the lower plate, and to reductions (up to 15%) on the inner side of the opposite upper plate. In particular, for $A/H = 0.69$, $\overline{Nu}_{1,i}$ attains a maximum value for every Ra number. On the other hand, $\overline{Nu}_{2,i}$ reaches a minimum value between $A/H = 0.38$ and 0.69, in the studied range of Ra numbers.

Attention may be now turned to per-plate heat transfer performance results. The per-plate convective conductance can be easily obtained from the ratio between the per-plate convective heat flux Q_c and the corresponding temperature drop $T_w - T_\infty$ in the steady state, without the aid of optical measurements. The above-defined per-plate conductance showed only slight variations on varying A/H from 0 to 1 for all the S/H and Ra values considered here. As expected from previous considerations on local data, the lower plate was found to take advantage of the vertical stagger, with reductions in wall temperatures and thus enhancement in heat transfer performance, but the extent of this enhancement turned out to be only 10% percent. On the other hand, the heat transfer performance of the upper plate was generally reduced by 10% at the most.

Another indication of the per-plate heat transfer performance can be obtained by averaging, for each plate, local Nusselt numbers on both vertical sides, which constitute 87% of the per-plate heat transfer surface area. Averaging local Nusselt numbers obtained by optical measurements also led to the same results, i.e. only minor differences (within $\pm$ 10–15%) in the per-plate heat transfer performance between the staggered and the unstaggered configurations, in spite of the strong influence exerted on local heat transfer characteristics. Indeed, the large heat transfer enhancement recorded, for instance, on the inner side of the lower plate is largely suppressed when the average between inner and outer side mean heat transfer coefficients is performed.

CONCLUSIONS

The present experiments provided basic data about the thermal field and the heat transfer characteristics of two staggered vertical plates cooled by air in free convection. The effects of the interplate spacing, the staggering magnitude, and the Rayleigh number were investigated.

As expected, the thermal field as well as the local

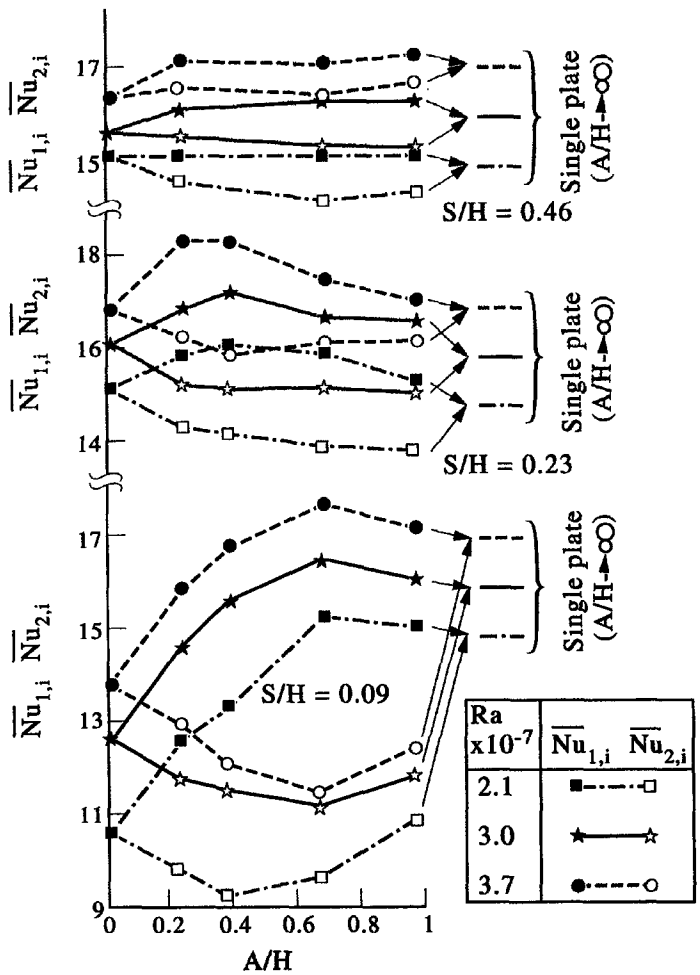

Fig. 10. Nusselt numbers $Nu_{1,i}$ (solid symbols) and $Nu_{2,i}$ (open symbols) averaged along the inner sides of plates 1 and 2 as a function of A/H, for different values of S/H and Ra.

heat transfer coefficients related to the outer sides of the two plates were found to be practically independent of the interplate spacing and the vertical staggering. Therefore, attention was mainly devoted to assessing the influence of the plate staggering on the local Nusselt numbers evaluated along the two inner facing sides of the plates. The extent to which local heat transfer performance was affected by the vertical stagger was found to be negligible or slight for intermediate and large interplate spacings.

For the lowest interplate spacing, appreciable differences between the unstaggered and the staggered cases were identified. In particular, the lower plate was found to take advantage of the vertical stagger of the opposite plate, with reductions in wall temperatures and enhancements of local heat transfer coefficients along the side facing the opposite plate. If only the facing sides (termed inner sides) of the plates are considered, the increase in heat transfer performance of the lower plate (as compared with the unstaggered configuration) can exceed 40%. Conversely, the heat transfer performance of the upper plate was found to be reduced by about 15% in the worst case.

When the entire per-plate surface area is taken into account, the effect of staggering in per-plate heat transfer performance is limited to $\pm 10\%$ at the most, even in the case of the smallest interplate distance, in spite of the large modifications induced in the local heat transfer.

REFERENCES

1. W. Elenbaas, Heat dissipation of parallel plates by free convection, *Physica* **9**, 1–28 (1942).
2. W. Elenbaas, Dissipation of heat by free convection. Part II, *Philips Res. Rep.* **3**, 450–465 (1948).
3. W. Aung, L. S. Flechter and V. Sernas, Developing laminar free convection between vertical flat plates with asymmetric heating, *Int. J. Heat Mass Transfer* **15**, 2293–2308 (1972).
4. J. R. Carpenter, D. G. Briggs and V. Sernas, Combined radiation and developing laminar free convection between vertical flat plates with asymmetric heating, *ASME J. Heat Transfer* **98**, 95–100 (1976).
5. E. M. Sparrow and P. A. Bahrami, Experiments on natural convection from vertical parallel plates with

either open or closed edges, *ASME J. Heat Transfer* **102,** 221–227 (1980).
6. R. A. Wirtz and R. J. Stutzman, Experiments on free convection between vertical plates with symmetric heating, *ASME J. Heat Transfer* **104,** 501–507 (1982).
7. D. Naylor, J. M. Floryan and J. D. Tarasuk, A numerical study of developing free convection between isothermal vertical plates, *ASME J. Heat Transfer* **113,** 620–626 (1991).
8. A. Bar-Cohen and W. M. Rohsenow, Thermally optimum spacing of vertical, natural convection cooled, parallel plates, *ASME J. Heat Transfer* **106,** 116–123 (1984).
9. N. Sobel, F. Landis and W. K. Mueller, Natural convection heat transfer in short vertical channels including the effects of stagger, *Proc. 3rd Int. Heat Transfer Conf.*, Vol. II, pp. 121–125 (1966).
10. E. M. Sparrow and C. Prakash, Enhancement of natural convection heat transfer by a staggered array of discrete vertical plates, *ASME J. Heat Transfer* **102,** 215–220 (1980).
11. C. Prakash and E. M. Sparrow, Natural convection heat transfer performance evaluations for discrete- (in-line or staggered) and continuous-plate arrays, *Numer. Heat Transfer* **3,** 89–105 (1980).
12. G. Guglielmini, E. Nannei and G. Tanda, Natural convection and radiation heat transfer from staggered vertical fins, *Int. J. Heat Mass Transfer* **30,** 1941–1948 (1987).
13. G. Tanda, Natural convection in partially heated vertical channels, *Wärme Stoffübert.* **23,** 307–312 (1988).
14. S. Acharya and D. S. Jang, Buoyancy-induced convection heat transfer in a staggered vertical channel, *Numer. Heat Transfer* **13,** 515–526 (1988).
15. G. Tanda, Natural convection heat transfer from a staggered vertical plate array, *ASME J. Heat Transfer* **115,** 938–945 (1993).
16. F. Devia, G. Milano and G. Tanda, Evaluation of thermal field in buoyancy-induced flows by a schlieren method, *Exp. Thermal Fluid Sci.* **8,** 1–9 (1994).
17. R. J. Moffat, Describing the uncertainties in experimental results, *Exp. Thermal Fluid Sci.* **1,** 3–17 (1988).
18. S. Ostrach, An analysis of laminar free-convection flow and heat transfer about a flat plate parallel to the direction of the generating body force, National Advisory Committee for Aeronautics Report No. 1111 (1953).